PAPER

Preparation and performance of electrically conductive Nb-doped TiO$_2$/polyaniline bilayer coating for 316L stainless steel bipolar plates of proton-exchange membrane fuel cells

Yanli Wang, [ID] [a] Shenghua Zhang, [b] Zhaoxia Lu,*[a] Ping Wang,[a] Xiaohong Ji[a] and Weihua Li [ID] *[ac]

A bilayer coating composed of an inner layer of Nb-doped TiO$_2$ obtained by the sol−gel method and an external polyaniline layer with small SO$_4^{2-}$ groups obtained by galvanostatic deposition was prepared to protect 316L stainless steel bipolar plates of proton-exchange membrane fuel cells. The corrosion resistances of bare 316L and 316L with single polyaniline coating and Nb-doped TiO$_2$/polyaniline bilayer coating were investigated. The experimental results indicated that both single and bilayer coatings increased the corrosion potential and decreased the corrosion current density compared with bare 316L stainless steel. A thirty-day exposure experiment indicated that the Nb-doped TiO$_2$/polyaniline bilayer showed high stability, and it protected 316L more effectively from the penetration of the corrosive ions.

1. Introduction

A bipolar plate is one of the important components in a proton-exchange membrane fuel cell (PEMFC), accounting for about 80% of the total weight and 45% of the stack manufacturing cost.[1] Among all the materials used as the bipolar plates, metallic bipolar plates have aroused increasing interest due to their higher strength, better processability and lower cost, which can greatly improve the power and energy density of PEMFC. However, the metallic bipolar plates exhibit dissolution and passivation in the acidic PEMFC environments.[2,3] The poor conductivity of the passivation film causes an increase in the contact resistance between the bipolar plate and the diffusion layer, thus decreasing the performance of the cell. The application of a conductive coating has been shown to be a simple and effective way to improve the corrosion resistance and the conductivity of the bipolar plates.

The conductive polymer coatings have received considerable attention as a kind of protective coating on the metallic bipolar plates because of their good conductivity, high thermal stability, simple synthetic process, smaller density and good corrosion resistance.[4–6] Since DeBerry[7] found that the polyaniline coatings on the stainless steel possess good corrosion resistance in the H$_2$SO$_4$ aqueous solution, the corrosion resistance and

mechanism of the conductive polymer coatings on the metallic substrates have been attracting significant attention. Up to now, conductive polymer coatings have been successfully used on metal bipolar plates.[8–13] Herrasti[8] found that the polypyrrole coating increased the corrosion potential and reduced the oxidation current density compared to bare stainless steel. Zhang[9] investigated the corrosion behavior of polypyrrole (Ppy) in HCl aqueous solution for fifty days. They reported that the Ppy coating not only increased the corrosion potential of the steel, but also significantly increased the pitting corrosion potential. Ren researched the corrosion resistance of polyaniline[10] and polyaniline/polypyrrole[11] coatings, and the results indicated that single polyaniline coating could decrease the corrosion rate by about two orders of magnitude, and a bilayer coating showed better corrosion resistance. The conductivity of the polymer coating is related to the doping ions. However, in an anodic PEMFC environment, the polymer coating is in a reductive state, which facilitates the de-doping reaction. This can result in the passivation of the substrate and the release of the doping ions from the polymer coating,[14] which limits the applications of the polymer coating in PEMFCs.

In the present study, an Nb-doped TiO$_2$ coating is prepared as the interlayer between 316L stainless steel and the polyaniline coating. The corrosion behaviors of the uncoated and coated 316L in H$_2$SO$_4$ solution were investigated.

[a] School of Chemistry and Chemical Engineering, Guangxi University, Nanning, 530004, P. R. China. E-mail: wyl187358@gxu.edu.cn

[b] School of Resources, Environment and Materials, Guangxi University, Nanning, 530004, P. R. China

[c] College of Chemical Engineering and Technology, Sun Yat-sen University, Zhuhai, 519082, P. R. China

2. Experimental procedures

A type of 316L stainless steel was used as the substrate alloy in the present study. The bulk materials were cut into specimens

with a size of 10 mm × 15 mm × 2 mm by an electric spark cutter, followed by grinding with 1000# grit emery paper, cleaning with distilled water and acetone, and then drying with an electric hair drier. The $Ti_{0.94}Nb_{0.06}O_2$ film was prepared by the sol–gel method. Tetrabutyl titanate and niobium(v) ethoxide were used as the raw materials for the sol. Acetyl acetone was used as a chelating agent, and ethanol was used as the solvent. The sol was aged for 12 h before spin-coating it on the 316L substrate. After the spin-coating process, the gel films were annealed at 500 °C at a heating rate of 4 °C min^{-1} for 2 h in air to obtain a stable $Ti_{0.94}Nb_{0.06}O_2$ film. Then, the bare 316L and $Ti_{0.94}Nb_{0.06}O_2$-coated-316L film specimens were embedded in an epoxy resin. For the preparation of the $Ti_{0.94}Nb_{0.06}O_2$/Pani bilayer coatings, a Pani layer doped with SO_4^{2-} was galvanostatically deposited on the $316L/Ti_{0.94}Nb_{0.06}O_2$ specimens at a current density of 3 mA cm^{-2} in a 0.5 M polyaniline + 1 M H_2SO_4 solution at 5 °C. For comparison, single Pani layer doped with SO_4^{2-} was electrodeposited on the bare 316L stainless steel in a solution of 0.5 M polyaniline and 1 M H_2SO_4 at 5 °C. Then, scanning electron microscopy (SEM), X-ray diffraction (XRD) and Fourier transform infrared spectroscopy (FTIR) were used to characterize the coatings.

For the electrochemical measurements, a three-electrode system was used; a Pt electrode was used as the counter electrode, and Ag/AgCl (saturated KCl) was used as the reference electrode. An accelerated corrosion test was performed in 0.1 M H_2SO_4 solution at 80 °C to rapidly evaluate the protection provided by the coatings to 316L. All electrochemical experiments including potentiodynamic polarization, open circuit potential and electrochemical impedance measurements were conducted with the Princeton Applied Research Versa STAT 4 potentiostat/galvanostat system. Potentiodynamic polarization was performed at a scan rate of 20 mV min^{-1} after 1 h immersion in the solution. Electrochemical impedance measurements were obtained at an open circuit potential between 0.01 Hz and 100 kHz, with the amplitude of input sine wave voltage of 10 mV.

3. Results and discussion

3.1. 1Characterization of the coatings

Fig. 1a shows the XRD pattern of the $Ti_{0.94}Nb_{0.06}O_2$ thin film coated onto 316L at an annealing temperature of 500 °C. The pattern reveals that the $Ti_{0.94}Nb_{0.06}O_2$ film consists of the anatase phase. Fig. 1b gives the cross-sectional morphology of $Ti_{0.94}Nb_{0.06}O_2$-coated 316L. It can be seen that the thickness of the $Ti_{0.94}Nb_{0.06}O_2$ film is about 0.64 μm. Furthermore, the adherence between the film and the substrate is good. Fig. 2 presents the potential-time dependence for the galvanostatic electrodeposition of Pani coatings on bare 316L and $Ti_{0.94}Nb_{0.06}O_2$-coated 316L specimens. Both the curves show the same changes and the presence of a potential peak, which may be related with the nucleated over-potential.[10] The potential is then stabilized at different constant values, which may be related to the growth of the Pani coatings on different surfaces. The thickness (d) of Pani is correlated with the electric quantity (Q), as shown in the following equation:
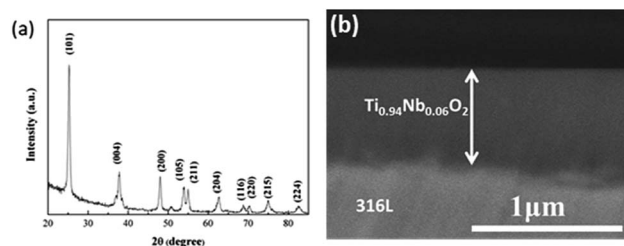

Fig. 1 XRD pattern (a) and the cross-sectional morphology (b) of the $Ti_{0.94}Nb_{0.06}O_2$ thin film at an annealing temperature of 500 °C.
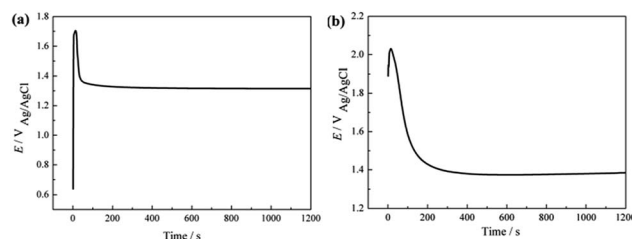

Fig. 2 Potential-time dependence for the galvanostatic electrodeposition of Pani coating on bare 316L (a) and $Ti_{0.94}Nb_{0.06}O_2$-coated 316L (b) specimens.

$$d = QM/2F\rho \qquad (1)$$

Therefore, the thickness of Pani in our experiment is about 18 μm.

The Pani coatings doped with sulfate ions deposited on 316L stainless steel and $Ti_{0.94}Nb_{0.06}O_2$ film were characterized by FTIR, as shown in Fig. 3. The FTIR spectra of Pani coated on the 316L stainless steel and the $Ti_{0.94}Nb_{0.06}O_2$ film showed the same characteristics. The peak at 790 cm^{-1} represented the out-of-plane bending vibration of a C–H bond on the benzene ring. The peak at 1225 cm^{-1} represented the bending vibration of a C=C bond on the quinone ring. The peak at 1295 cm^{-1} represented the stretching vibration of a secondary amine (C–N) connected to the benzene ring. The peaks at 1473 and 1560 cm^{-1} represented the characteristics of the quinoid ring
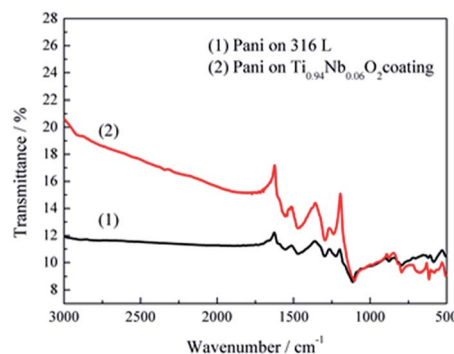

Fig. 3 FTIR spectra of the Pani coating doped with sulfate ions deposited on 316L stainless steel and the $Ti_{0.94}Nb_{0.06}O_2$ film.
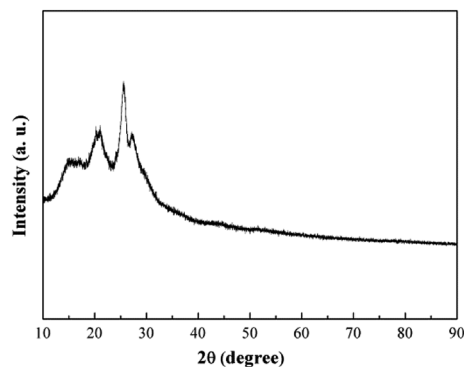
Fig. 4 XRD pattern of the polyaniline coating on 316L.

and the benzene ring in the polyaniline, respectively. The peak at 1115 cm^{-1} represented the antisymmetric stretching vibration of SO_4^{2-}, indicating the successful doping of protonic acid. These typical peaks were in accordance with the main peaks of Pani reported previously.[15]

The XRD pattern of Pani deposited on 316L is shown in Fig. 4. Some peaks appeared due to the local crystallinity of Pani, which may be caused by the periodicity perpendicular to the polymer chain.[16] The SEM images of 316L with the single polyaniline coating and $Ti_{0.94}Nb_{0.06}O_2$/polyaniline bilayer coating are presented in Fig. 5, and they showed that both Pani coatings were porous. The Pani coating deposited on 316L was slightly smoother than that deposited on the $Ti_{0.94}Nb_{0.06}O_2$ film.

3.2 Free corrosion potential

Fig. 6 presents the free corrosion potentials for bare 316L and 316L with Pani and $Ti_{0.94}Nb_{0.06}O_2$/Pani coatings in 0.1 M H_2SO_4 solution bubbled with air at 80 °C for 720 h. For bare 316L, E_{corr} increases with time in the initial 25 h and then decreases slowly after immersion for 240 h. E_{corr} for the single Pani coating increases slowly to around 220 mV$_{Ag/AgCl}$ at the initial stage, which may be related to the passivation of the 316L substrate.[10] However, E_{corr} decreases slowly after immersion for 240 h, reaching a value of about 155 mV$_{Ag/AgCl}$, which is still higher than that for the bare 316L; the same trend can be seen for the Pani-coated type 304 steel, as reported by Ren.[10] This can be related to the inward penetration of the solution into the coating. Unlike the observations for the single Pani coating,
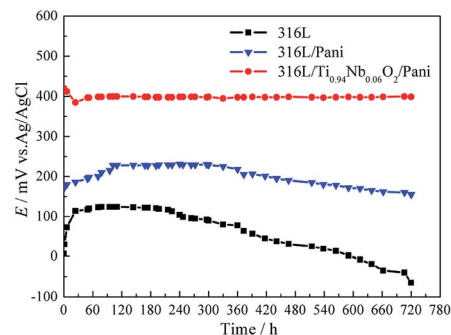

Fig. 5 The SEM images of 316L with single polyaniline coating and Nb-doped TiO_2/polyaniline bilayer coating.

Fig. 6 Free corrosion potentials for bare 316L and 316L with Pani and $Ti_{0.94}Nb_{0.06}O_2$/Pani coatings in 0.1 M H_2SO_4 solution bubbled with air at 80 °C for 720 h.

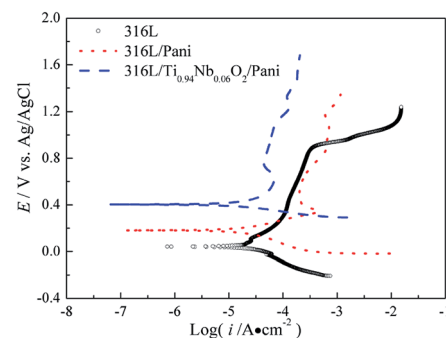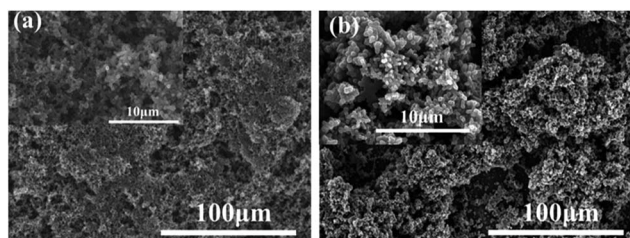**Fig. 7** Potentiodynamic polarization curves of 316L and 316L with Pani and $Ti_{0.94}Nb_{0.06}O_2$/Pani coatings after immersion in 0.1 M H_2SO_4 solution bubbled with air at 80 °C for 1 h.

E_{corr} for the $Ti_{0.94}Nb_{0.06}O_2$/Pani coating is almost constant at around 400 mV$_{Ag/AgCl}$ during the 720 h immersion in 0.1 M H_2SO_4 solution. Both the Pani coating and the $Ti_{0.94}Nb_{0.06}O_2$/Pani coating can improve the corrosion potential of the bare 316L, thus providing anodic protection for 316L, which is similar to the result reported in.[17] It can be indicated that the bilayer coating is more protective than the single Pani coating.

3.3 Potentiodynamic polarization measurements

Fig. 7 gives the potentiodynamic polarization curves of 316L and 316L with Pani and $Ti_{0.94}Nb_{0.06}O_2$/Pani coatings after immersion in 0.1 M H_2SO_4 solution bubbled with air at 80 °C

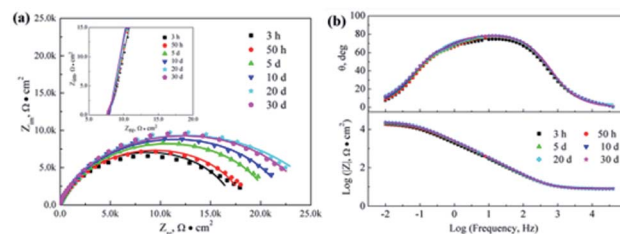**Fig. 8** Nyquist and Bode plots for the corrosion of 316L potentiostatically polarized at +600 mV$_{Ag/AgCl}$ in 0.1 M H_2SO_4 solution bubbled with air at 80 °C for various time durations. Symbol: experimental data; line: simulation data.
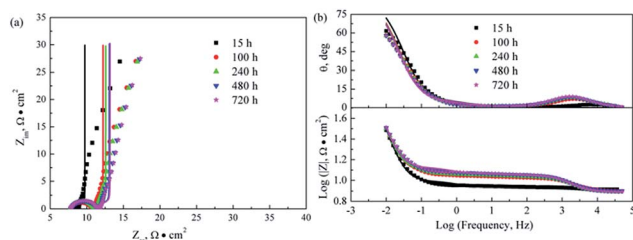
Fig. 9 Nyquist and Bode plots for the corrosion of 316L with Pani coating potentiostatically polarized at +600 mV$_{Ag/AgCl}$ in 0.1 M H$_2$SO$_4$ solution bubbled with air at 80 °C for various lengths of time. Symbol: experimental data; line: simulation data.

Fig. 10 Nyquist and Bode plots for the corrosion of 316L with Ti$_{0.94}$Nb$_{0.06}$O$_2$/Pani coating potentiostatically polarized at +600 mV$_{Ag/AgCl}$ in 0.1 M H$_2$SO$_4$ solution bubbled with air at 80 °C for various lengths of time. Symbol: experimental data; line: simulation data.
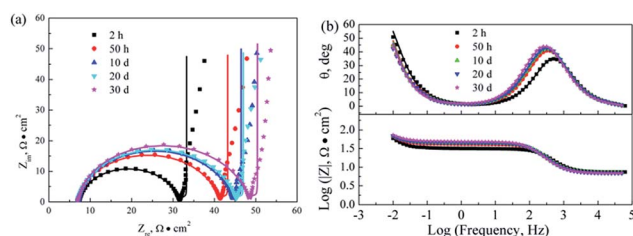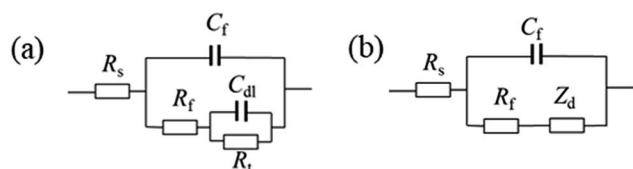

Fig. 11 Equivalent circuit for fitting the impedance spectra of the bare 316L (a) and 316L with Pani and Ti$_{0.94}$Nb$_{0.06}$O$_2$/Pani coatings (b).

for 1 h. The corrosion potential and corrosion current density for bare 316L are around 46 mV$_{Ag/AgCl}$ and 24 μA cm^{-2}, respectively, which are obtained by the cathodic Tafel extrapolation, whereas those for 316L with Pani coating are approximately 184 mV$_{Ag/AgCl}$ and 20 μA cm^{-2}, and those for 316L with Ti$_{0.94}$Nb$_{0.06}$O$_2$/Pani bilayer coating are about 400 mV$_{Ag/AgCl}$ and 13.8 μA cm^{-2}. Thus, the Ti$_{0.94}$Nb$_{0.06}$O$_2$/Pani

bilayer coating causes a positive shift of more than 210 mV$_{Ag/AgCl}$ in the corrosion potential relative to the Pani coating. The corrosion current density for the bilayer coating is lower than that for the single Pani coating. Additionally, 316L suffers from transpassive dissolution at potentials higher than around 0.9 V, whereas the Pani- and Ti$_{0.94}$Nb$_{0.06}$O$_2$/Pani-coated steels exhibit wider passive regions. These results suggest that the coatings can effectively protect the bare 316L steel from the corrosion of the H$_2$SO$_4$ solution.

3.4 Electrochemical impedance spectra at the cathode potential

Fig. 8–10 show the Nyquist and Bode plots for the corrosions of 316L and 316L with Pani and Ti$_{0.94}$Nb$_{0.06}$O$_2$/Pani coatings potentiostatically polarized at +600 mV$_{Ag/AgCl}$ in 0.1 M H$_2$SO$_4$ solution bubbled with air at 80 °C for various lengths of time. The Nyquist plots for the bare 316L consist of two depressed capacitive loops (Fig. 8a). Although the two capacitive loops cannot be distinguished well, the plots of the phase angle clearly show two time constants (Fig. 8b). The capacitive loops at low frequencies expand with the increasing immersion time, which corresponds to the passivation of the 316L substrate. The plots at the high frequency section represent the behavior of the film, and those in the low frequency section indicate the response to the electrochemical reaction at the interface between the film and the substrate. Unlike the observations for 316L, the Nyquist plots for the corrosion of the coated steels show a small capacitive loop at high frequencies and a line at low frequencies instead of two depressed capacitive loops (Fig. 9 and 10). The line is almost perpendicular to the real axis, probably suggesting an effective barrier behavior. The impedance spectra of 316L can be fitted by the equivalent circuit shown in Fig. 11a, and those of 316L with Pani and Ti$_{0.94}$Nb$_{0.06}$O$_2$/Pani coatings can all be fitted by the equivalent circuit shown in Fig. 11b. In Fig. 11, R_s represents the solution resistance, C_{dl} and R_t represent the double-layer capacitance and charge transfer resistance, C_f and R_f represent the capacitance and resistance of the porous corrosion product layer or coatings, respectively, and Z_d represents the diffusion impedance of the barrier layer. The impedance, Z_d, is expressed as follows:

$$Z_d = T(jw)^{-1/2} \mathrm{Coth}[t(jw)^{1/2}] \qquad (2)$$

Table 1 Fitting results of impedance spectra for the corrosion of 316L in 0.1 M H$_2$SO$_4$ solution at 80 °C

Time (h)	R_s (Ω cm^2)	Y_f (Ω^{-1} cm^{-2} S^{-n})	n_f	R_f (Ω cm^2)	Y_{dl} (Ω^{-1} cm^{-2} S^{-n})	n_{dl}	R_t (Ω cm^2)
1	7.84	9.38×10^{-5}	0.88	0.67×10^4	4.08×10^{-5}	0.89	1.07×10^4
3	7.87	7.68×10^{-5}	0.90	0.69×10^4	6.25×10^{-5}	0.78	1.20×10^4
15	7.90	7.56×10^{-5}	0.90	0.77×10^4	6.99×10^{-5}	0.84	1.06×10^4
50	7.93	7.39×10^{-5}	0.90	0.87×10^4	6.40×10^{-5}	0.82	1.13×10^4
100	7.93	7.39×10^{-5}	0.90	0.87×10^4	7.07×10^{-5}	0.84	1.06×10^4
150	7.90	7.26×10^{-5}	0.90	0.89×10^4	6.57×10^{-5}	0.77	1.21×10^4
240	7.95	7.12×10^{-5}	0.90	0.95×10^4	6.16×10^{-5}	0.76	1.30×10^4
360	7.94	6.96×10^{-5}	0.90	1.02×10^4	5.99×10^{-5}	0.67	1.52×10^4
480	7.93	6.95×10^{-5}	0.90	1.03×10^4	6.55×10^{-5}	0.70	1.40×10^4
720	7.90	6.97×10^{-5}	0.90	1.16×10^4	8.03×10^{-5}	0.90	1.01×10^4

Table 2 Fitting results of impedance spectra for the corrosion of 316L with Pani coating in 0.1 M H_2SO_4 solution at 80 °C

Time (h)	R (Ω cm^2)	Y_f (Ω^{-1} cm^{-2} s^n)	n_f	R_f (Ω cm^2)	T (Ω^{-1} cm^{-2} s$^{0.5}$)	t (s$^{0.5}$)
3	7.447	4.88×10^{-4}	0.7179	0.735	0.2735	1.577
15	7.719	2.03×10^{-4}	0.8147	1.014	0.2735	1.577
50	7.331	2.38×10^{-4}	0.8205	1.687	0.3344	1.59
100	7.721	8.06×10^{-5}	0.9029	2.092	0.4036	1.28
150	7.845	8.31×10^{-5}	0.8983	2.549	0.4015	1.264
240	7.845	8.41×10^{-5}	0.896	2.81	0.3934	1.284
360	7.775	7.04×10^{-5}	0.915	3.023	0.3167	1.69
480	7.942	7.01×10^{-5}	0.9138	3.355	0.3025	1.738
720	7.815	7.30×10^{-5}	0.9102	3.413	0.3013	1.75

Table 3 Fitting results of impedance spectra for the corrosion of 316L with $Ti_{0.94}Nb_{0.06}O_2$/Pani coating in 0.1 M H_2SO_4 solution at 80 °C

Time (h)	R (Ω cm^2)	Y_f (Ω^{-1} cm^{-2} s^n)	n_f	R_f (Ω cm^2)	T (Ω^{-1} cm^{-2} s$^{0.5}$)	t (s$^{0.5}$)
2	7.36	4.19×10^{-5}	0.94	23.55	0.2171	1.544
15	7.06	4.83×10^{-5}	0.94	30.59	0.2102	1.552
50	7.10	4.96×10^{-5}	0.94	33.55	0.2074	1.602
100	7.04	5.10×10^{-5}	0.94	34.83	0.2111	1.524
150	7.09	5.19×10^{-5}	0.94	36.68	0.1984	1.610
240	6.98	5.34×10^{-5}	0.94	37.12	0.1976	1.637
360	6.97	5.44×10^{-5}	0.94	37.54	0.2105	1.554
480	6.99	5.76×10^{-5}	0.93	40.28	0.196	1.637
720	6.96	5.89×10^{-5}	0.93	40.76	0.1955	1.580

In the fitting procedure, a constant phase angle element (CPE) Q_{dl} is used to replace the element C_{dl}. The impedance of CPE is expressed as follows:

$$Z_{CPE} = Y_0^{-1} (jw)^{-n} \qquad (3)$$

According to the equivalent circuit shown in Fig. 11, the impedance spectra for the corrosion of the samples have been fitted, and some electrochemical parameters are listed in Tables 1–3.

Table 1 indicates that R_t for the corrosion of 316L is around 10^4 Ω cm^2 and hardly changes with the increase in the exposure time, indicating that 316L is in a steady corrosion state. R_f increases gradually with the immersion time from 0.67×10^4 to 1.16×10^4 Ω cm^2, corresponding to the formation of a passive film on the substrate during the immersion. Tables 2 and 3 indicate that the value of R_f for the corrosion of the $Ti_{0.94}Nb_{0.06}O_2$/Pani bilayer coating is approximately one order of magnitude larger than that of the single Pani coating, indicating better corrosion resistance. However, R_f for the bilayer coating is slightly larger than that for the single coating. The SO_4^{2-} ion doping reaction can occur easily at +600 mV$_{Ag/AgCl}$. In this system, the corrosion of the single Pani coating exhibits an effective barrier behavior. The corrosion potential for the bilayer is much higher than that for the single Pani layer; the whole corrosion process of the bilayer is controlled by the diffusion of corrosive ions between the Pani and $Ti_{0.94}Nb_{0.06}O_2$ coatings. The presence of the inner $Ti_{0.94}Nb_{0.06}O_2$ coating increases the diffusion distance of the corrosive ions. All the results indicate that the $Ti_{0.94}Nb_{0.06}O_2$/Pani bilayer coating can more effectively protect 316L than the single Pani coating.

4. Conclusions

Bilayer coatings consisting of an inner $Ti_{0.94}Nb_{0.06}O_2$ layer and an outer Pani layer are prepared on a 316L substrate for use as bipolar plates in proton-exchange membrane fuel cells. The bilayer coating increases the corrosion potential by more than 350 mV$_{Ag/AgCl}$. Moreover, the bilayer coating decreases the corrosion current density of bare 316L from 24 to 13.8 μA cm^{-2}. Potentiostatic polarization at +600 mV$_{Ag/AgCl}$ in 0.1 M H_2SO_4 solution at 80 °C for 720 h occurs at around 400 mV$_{Ag/AgCl}$, confirming the high stability and good corrosion resistance of the bilayer coating. The electrochemical impedance spectra of the bilayer consist of a small capacitive loop at high frequencies and a line at low frequencies, suggesting an effective barrier behavior.

Conflicts of interest

There are no conflicts to declare.

Acknowledgements

Notes and references

1 B. Cunningham and D. G. Baird, *J. Mater. Chem.*, 2006, **16**, 4385.

2 I. S. Lee, J. S. Kim, S. T. Kim, J. H. Kim and Y. Y. Lee, *Corros. Sci.*, 2013, **70**, 93.

3 H. Tawfik, Y. Hung and D. Mahajan, *J. Power Sources*, 2007, **163**, 755.

4 S. Biallozor and A. Kupniewska, *Synth. Met.*, 2005, **155**, 443.

5 H. Hammache, L. Makhloufi and B. Saidani, *Corros. Sci.*, 2003, **45**, 2031.

6 A. T. Ozyilmaz, M. Erbil and B. Yazici, *Thin Solid Films*, 2006, **496**, 431.

7 D. W. DeBerry, *J. Electrochem. Soc.*, 1985, **132**, 1022.

8 P. Herrasti and P. Ocon, *Appl. Surf. Sci.*, 2001, **172**, 276.

9 T. Zhang and C. L. Zeng, *Electrochim. Acta*, 2005, **50**, 4721.

10 Y. J. Ren, J. Chen and C. L. Zeng, *J. Power Sources*, 2010, **195**, 1914.

11 Y. J. Ren and C. L. Zeng, *J. Power Sources*, 2008, **182**, 524.

12 S. Joseph, J. C. McClure, R. Chianeli, P. Pich, P. Pich and P. J. Sebastian, *Int. J. Hydrogen Energy*, 2005, **30**, 1339.

13 M. A. Lucio Garcia and M. A. Smit, *J. Power Sources*, 2006, **158**, 397.

14 S. Sathiyanarayanan, V. Karpakam, K. Kamaraj, S. Muthukrishnan and G. Venkatachari, *Surf. Coat. Technol.*, 2010, **204**, 1426.

15 J. F. Pagotto, F. J. Recio, A. J. Motheo and P. Herrasti, *Surf. Coat. Technol.*, 2016, **289**, 23.

16 T. Abdirgrim, Z.-X. gang and R. Jamal, *Mater. Chem. Phys.*, 2005, **90**, 367.

17 P. J. Kinlen, D. C. Silverman and C. R. Jeffreys, *Synth. Met.*, 1997, **85**, 1327.